



Original Research Paper

Superior capacitive behavior of porous activated carbon tubes derived from biomass waste-cotonier strobili fibers

Xiao-Li Su ^{a,1}, Shuai-Hui Li ^{a,1}, Shuai Jiang ^a, Zhi-Kun Peng ^{a,*}, Xin-Xin Guan ^{a,b}, Xiu-Cheng Zheng ^{a,b,*}^a College of Chemistry and Molecular Engineering, Zhengzhou University, Zhengzhou 450001, China^b Key Laboratory of Advanced Energy Materials Chemistry (Ministry of Education), Nankai University, Tianjin 300071, China

ARTICLE INFO

Article history:

Received 30 March 2018

Received in revised form 13 May 2018

Accepted 16 May 2018

Available online 25 May 2018

Keywords:

Cotonier strobili fibers

Activated carbon tube

Hierarchical porous structure

Electrochemical behavior

Supercapacitors

ABSTRACT

As supercapacitor electrode materials, the sustainable biomass-derived activated carbons have attracted a great deal of attentions due to their low-cost, abundant, and unwanted natural wastes. In this work, a facile KOH activation method is adopted to prepare activated carbon tubes from the biomass waste-cotonier strobili fibers for the first time. The resultant PTAC-x materials possess highly accessible surface areas and abundant micro-mesopores, which benefit large ion storage and high-rate ion transfer. The optimized material denoted as PTAC-6 demonstrates a high specific capacity (346.1 F g^{-1} at 1 A g^{-1}) and a superior rate performance (214.5 F g^{-1} at 50 A g^{-1}) in the three-electrode supercapacitors. In addition, the symmetric supercapacitor exhibits excellent cycling stability with a capacitance retention of 84.21% and a columbic efficiency of nearly 100% after 10,000 cycles. Furthermore, the PTAC-6-based symmetric supercapacitor gives a remarkable specific energy of 33.04 Wh kg^{-1} at 160 W kg^{-1} . Meanwhile, our proposed porous activated carbon tubes provide a green and low-cost electrode material for high-performance supercapacitors.

© 2018 The Society of Powder Technology Japan. Published by Elsevier B.V. and The Society of Powder Technology Japan. All rights reserved.

1. Introduction

The human being is facing serious energy crisis, and the clean, efficient, sustainable and cheap energy-storage device is thus urgent. As one of the most promising energy storage devices, supercapacitor has received extensive attention due to their high power density, fast charge and discharge rates, and long-term cycling stability, etc. [1–8]. Compared with the pseudo-capacitors based on quick and reversible Faradaic redox reaction on the surface and bulk structure of metal oxides, the electrical double layer capacitors (EDLCs) dependent on the electrostatic interaction between the ions on surface area of the electrode materials and electrolytes, are a more commonly mode for energy storage. However, the intrinsic low energy density limits the practical application in energy-efficient industrial equipment [9,10].

Activated carbon (AC) is a common electrode material for many electrochemical storage systems owing to its high surface area, abundant porosity, efficient electrical & thermal conductivity, high

stability, availability, and cost-effective [11]. At present, the main raw materials for ACs are classified into three types: (1) Organic polymer including phenolic resin, polysaccharide, etc.; (2) Plants, such as fruit shells, wood chips, ramie; and (3) Derivatives of coal and its mixtures. Biomass outperforms the other materials due to their cost-effective, environmentally friendly as well as readily available in high quality and quantity properties. Notably, the basic components of plant biomass (cellulose, hemicellulose, lignin, plant protein, plant lipids, etc.) offer a basic skeleton structure and abundant functional groups for the carbons [12]. Especially, the biomass consisting of 3D interconnected network with open pores facilitates the fast ionic and electronic diffusion and transmission. As a result, the biomass has a potential as superior electrode materials for supercapacitors.

Till now, various biomasses such as camellia oleifera shell [13], cotton, cotton-flax, and flax fabrics [14], ginkgo leaves [15], elm samara [16], bagasse [17], poplar catkins [18], corncob [19], and rice husk ash [20] have been used to prepare AC electrode materials for supercapacitors. Cotonier strobili are the fruits of cotonier (also called as plane tree). As shown in Fig. 1, they are formed by small nuts surrounded by cotonier strobili fibers. One cotonier strobili has 600–1400 small nuts and one small nut have roughly 3000 cotonier strobili fibers. When cotonier strobili are matured, the lightweight fibers fly around, leading to the serious environ-

* Corresponding authors at: College of Chemistry and Molecular Engineering, Zhengzhou University, Zhengzhou 450001, China (X.-C. Zheng).

E-mail addresses: zhikumpeng@163.com (Z.-K. Peng), zhxch@zzu.edu.cn (X.-C. Zheng).

¹ X.L. Su and S.H. Li contributed equally to this work.

mental pollution, and harm people's health through a variety of pathways including skin irritation, or respiratory tract, etc. Although cotonier strobili fibers containing abundant cellulose have low economic value, the cotonier strobili fibers with hollow

structure can be converted into ACs with interconnected networks as well as relatively high electrical conductivity. The converted ACs from cotonier strobili fibers are expected to possess superior electrochemical properties.

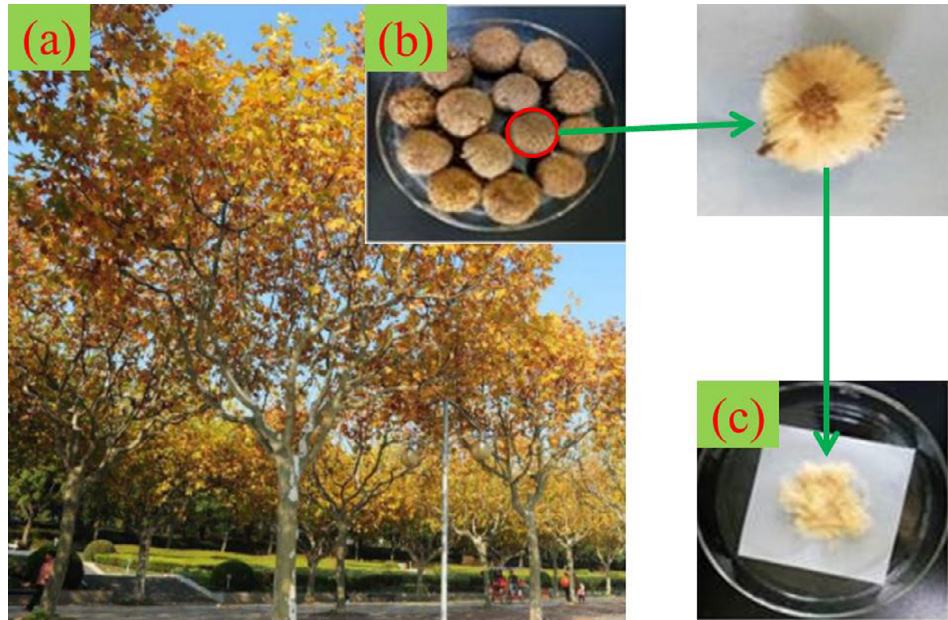


Fig. 1. Photos of cotonier (a), cotonier strobile (b) and cotonier strobile fibers (c).

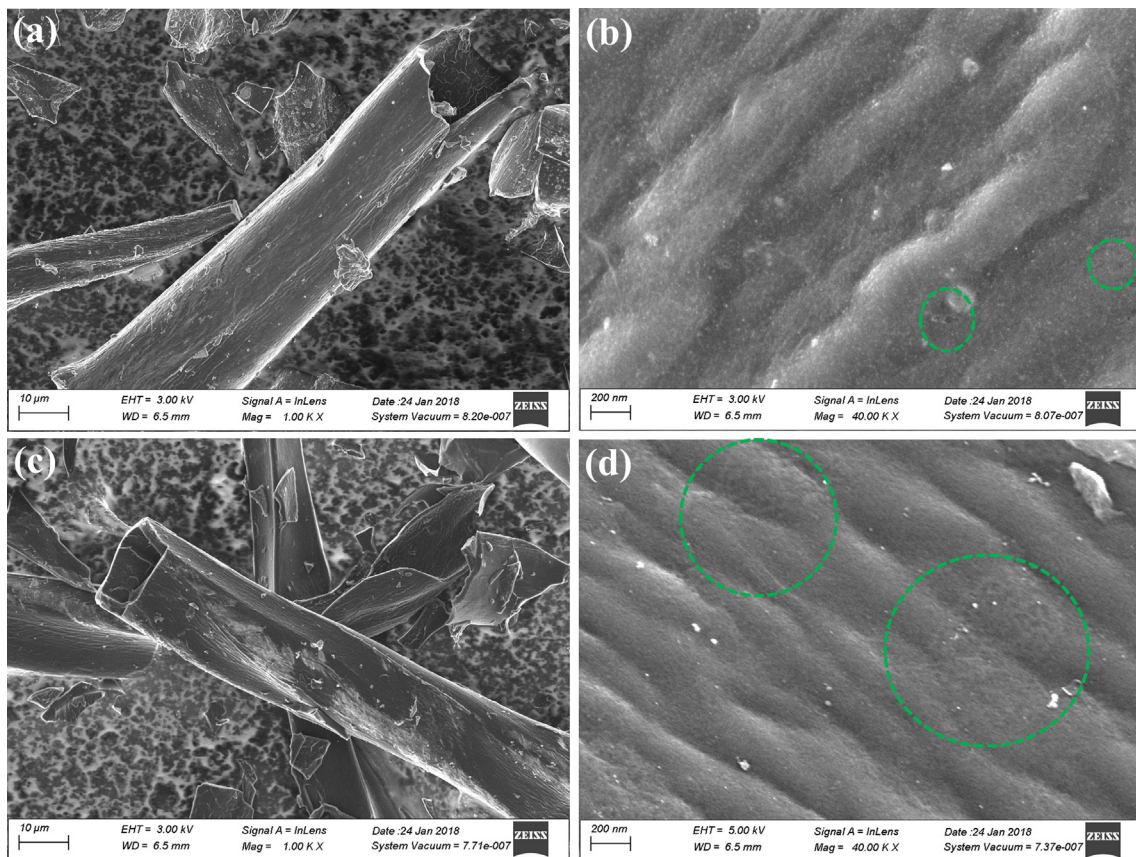


Fig. 2. SEM images PTC (a, b) and PTAC-6 (c, d).

In this work, a KOH chemical activation method is used to prepare 3D hierarchical porous carbon tubes from the biomass waste-cotonier strobili fibers. The resultant AC materials display excellent capacitive behavior, demonstrating an efficient strategy for high-performance supercapacitor electrode materials.

2. Experimental

2.1. Pretreatment of the raw material

Cotonier strobili were collected in Zhengzhou University in December 2016. The fibers reserved from cotonier strobili were dispersed into ethanol under violent stirring to remove the impurities and washed by deionized (DI) water. Subsequently, they were dealt with dilute HNO_3 solution for 12 h, washed with DI water, and dried in an oven.

2.2. Synthesis of the porous carbon tube materials

2 g of the pretreated cotonier strobili fibers was pre-carbonized at 600 °C for 4 h in N_2 atmosphere ($5 \text{ }^{\circ}\text{C min}^{-1}$). The resultant materials were denoted as PTC. PTC was further impregnated with KOH solution, heated at 80 °C to evaporate water, and calcined at 800 °C for 1 h in N_2 atmosphere ($5 \text{ }^{\circ}\text{C min}^{-1}$). The samples were treated with HCl solution (1 M), washed with DI water, and dried in an oven. The resultant activated carbons were denoted as PTAC-x (x referred to the mass ratios for the dosage of KOH to PTC, which was 2, 4, 6, or 8).

2.3. Characterization of the materials

The microstructures of the samples were carried out on a Zeiss Ultra 55 scanning electron microscope (SEM) and a FEI-TalosF200S transmission electron microscope (TEM). Their phase structures were examined by X-ray diffraction (XRD) on a Panalytical X'pert-Pro diffractometer operated at 40 kV and 40 mA using $\text{Cu K}\alpha$ radiation ($\lambda = 0.15406 \text{ nm}$). The textural parameters were demonstrated by nitrogen adsorption-desorption isotherms at $-196 \text{ }^{\circ}\text{C}$ using a Micromeritics ASAP 2420-4MP automated surface area and pore size analyzer. The specific surface area was calculated by the Brunauer-Emmett-Teller (BET) method. Density functional theory (DFT) model assuming cylindrical-shaped pores was utilized to obtain the pore size distribution from the desorption isotherms. Raman spectra were carried out on a LabRAM HR Evolution Raman spectrometer. Surface chemistry was investigated by X-ray photoelectron spectroscopy (XPS) using an RBD upgraded PHI-5000C ESCA system (Perkin Elmer) and the binding energies were calibrated using the containment carbon (C 1s = 284.6 eV).

2.4. Tests of the electrochemical performance of the materials in the three- and two-electrode supercapacitor systems

The three-electrode configurations were employed to evaluate the capacitive properties of the as-prepared carbon materials in 6 mol L^{-1} KOH electrolyte solution on a CHI 660E electrochemical workstation (Shanghai Chenhua Instruments Co., China). A platinum electrode and an Ag/AgCl electrode were acted as counter

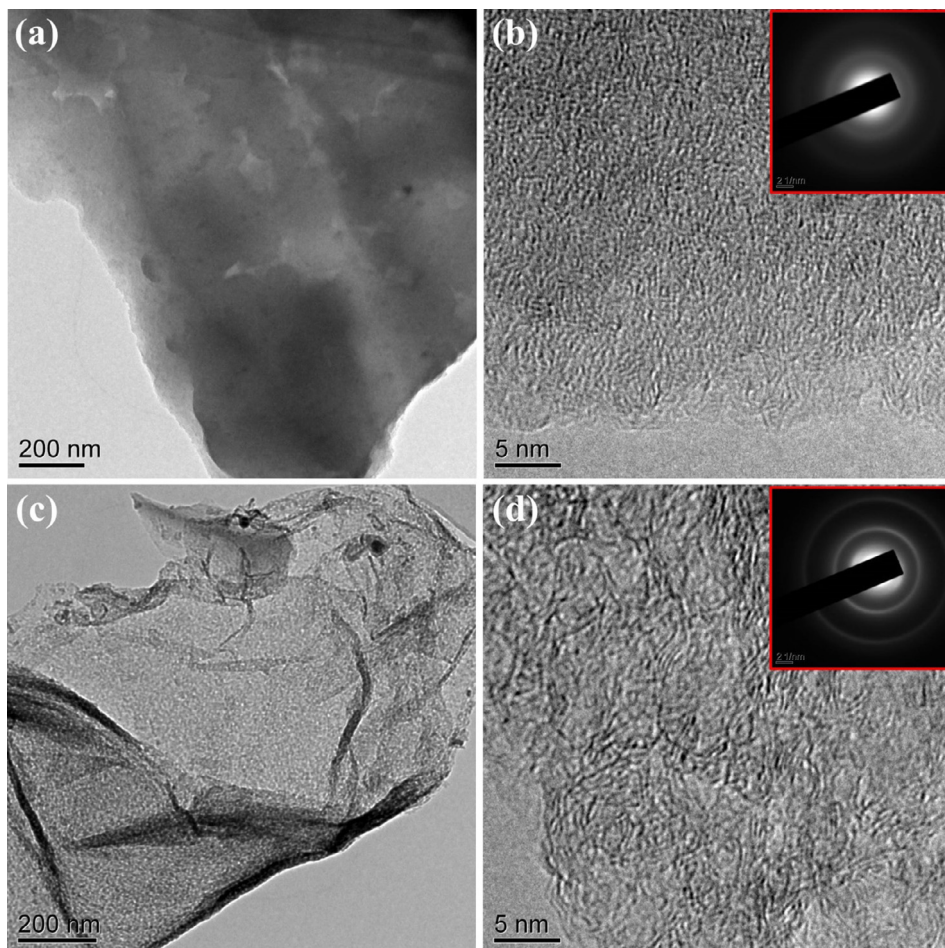


Fig. 3. TEM images of PTC (a, b) and PTAC-6 (c, d); SAED patterns of PTC (inset of b) and PTAC-6 (inset of d).

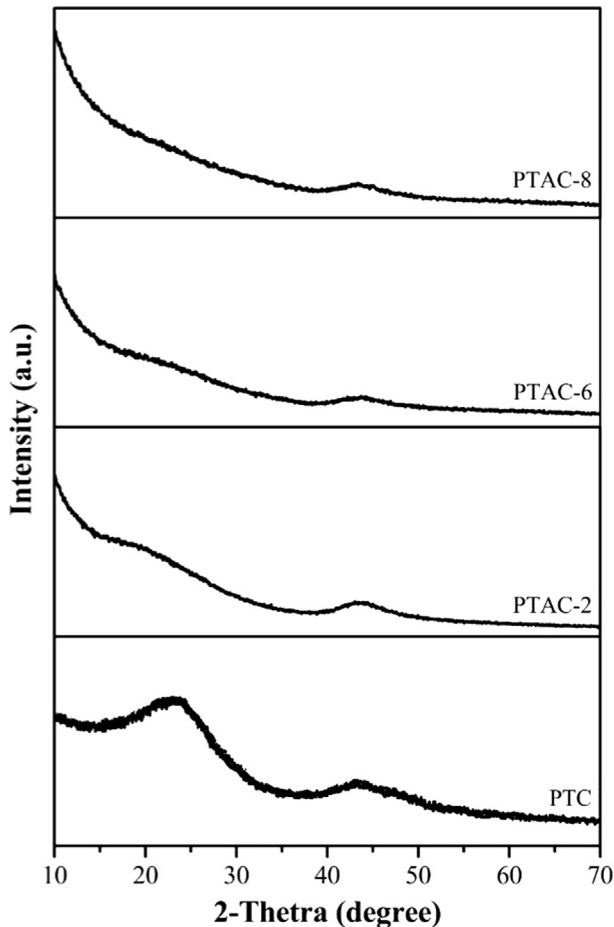


Fig. 4. XRD patterns of PTC and PTAC-x.

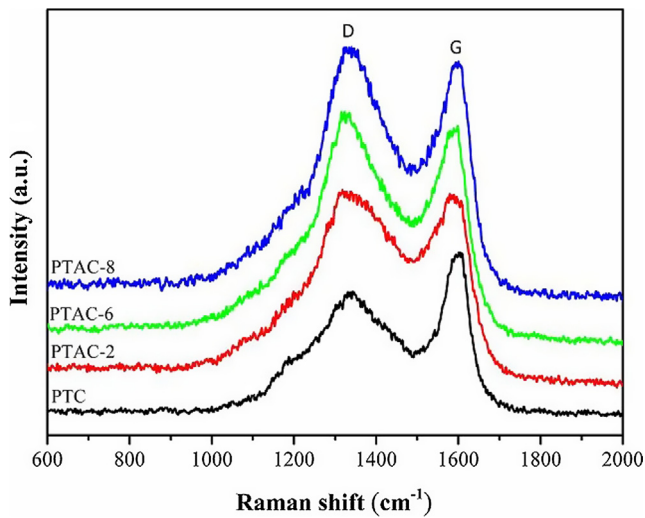


Fig. 5. Raman spectra of PTC and PTAC-x.

and reference electrodes, respectively. In addition, several strategies were adopted to keep the stability of the used Ag/AgCl electrode in the alkaline electrolyte, such as using leakless electrode, shorting exposure to the electrolyte, and frequent exchange of filling solution. The working electrode was prepared with a mixture of 80 wt% active material, 10 wt% conductive acetylene black, and 10 wt% polytetrafluoroethylene (PTFE) in ethanol solution. The uniformly ground slurry was coated on a nickel foam sheet (1×1

cm^2), dried at 60°C under vacuum overnight, and pressed at 10 MPa for 30 s. The mass loading of the active materials in each working electrode was about 2 mg cm^{-2} . The cyclic voltammetry (CV) tests were carried out in a potential range of -1 to 0 V with scan rates of 5 – 100 mV s^{-1} . Electrochemical impedance spectroscopy (EIS) tests were investigated over a frequency range of 100 kHz to 0.01 Hz at the open circuit potential. The specific capacitance (C_m) was calculated from the galvanostatic charge-discharge (GCD) values by using Eq. (1),

$$C_m = \frac{I \times \Delta t}{\Delta V \times m}. \quad (1)$$

where I , Δt , m , and ΔV were discharge current (A), discharge time (s), the total mass of the active material (g) in work electrodes, and the voltage change (V) excluding the IR drop during the discharge process, respectively.

In a two-electrode system, the symmetric supercapacitors were assembled using two exactly the same mass electrodes with a filter paper soaked in Na_2SO_4 solution (1 M) and CR-2016 model battery jar were used as current collector. The GCD and CV tests were performed in the potential range of 0 – 1.6 V . The specific capacitance of the two-electrode system calculated from GCD was similar with the aforementioned three-electrode system. The specific energy density (E , Wh kg^{-1}) and specific power density (P , W kg^{-1}) in the two-electrode system were calculated by using Eqs. (2) and (3), respectively.

$$E = \frac{1}{2} C_m \times V^2 \quad (2)$$

$$P = \frac{E}{t} \quad (3)$$

where V (V) was the cell voltage for charging and discharging and t (h) was the discharge time.

3. Results and discussion

3.1. Material characterization

As revealed by SEM images, the as-prepared PTC exhibits a hollow microtubular structure with a diameter of about $10 \mu\text{m}$ and the wall thickness is less than $1.5 \mu\text{m}$ (Fig. 2a). Fig. 2b shows that there are few mesopores on the outer coarse surface of PTC due to the gas-state substances escaping during carbonization process. PTAC-6 remains the hollow microtubular structure of PTC even after the calcination and activation process (Fig. 2c). Additionally, compared with that of PTC, there are much more mesopores on the tube wall of PTAC-6, which are mainly originated from the KOH chemical etching.

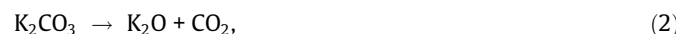
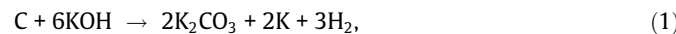
The microspores produced from the KOH etching are not obvious in the typical SEM images limited by the magnification [21,22]. The TEM images of PTC and PTAC-6 are provided more clearly magnified images (Fig. 3). Fig. 3c reveals that there are abundant pores on the tube walls of PTAC-6, which stems from the evaporation of H_2O and CO_2 during the pyrolysis of cotonier strobili fibers and the chemical etching of KOH. Compared with PTC, PTAC-6 possesses a thinner and smoother surface (Fig. 3c), which comes from the destruction of the surface morphology of PTC by the etching of KOH. The specific characteristic of tube and pores form a unique 3D porous architecture and lead to an increased surface area. It is distinctly observed that PTAC-6 appears obviously looser than PTC. In addition, their selected area electron diffraction (SAED) patterns inserted in Fig. 3b and d demonstrate their nature of carbon materials.

The XRD pattern of PTC shown in Fig. 4 reveals two obvious peaks at ca. 23° and 43° that can be indexed to the (0 0 2) and

(1 0 0) planes of the disordered carbon layer, respectively [23]. The intensities of these peaks, especially for that of (0 0 2), become gradually weaker with increasing of KOH dosage in the patterns of PTAC- x . This indicates the existence of structural defects because of the randomly oriented aromatic carbon sheets in these materials. These defects facilitate generating high surface area and the highly porous structure [24–26].

PTC and PTAC- x exhibit two characteristic Raman bands at 1350 cm^{-1} (D-band) and 1580 cm^{-1} (G-band) (Fig. 5). The intensity ratios of D and G bands (I_D/I_G) for PTAC- x (~ 1.08) are obviously higher than that of PTC ($I_D/I_G = 0.74$), demonstrating that PTAC- x have more disordered and defective carbons than PTC due to the exposure of edges during the pore evolution process.

N_2 adsorption-desorption was conducted to investigate the textural parameters of the resultant carbons. As shown in Fig. 6a, the PTAC- x materials ($x = 2, 6$, and 8) show much larger N_2 adsorption volume than PTC, implying they have higher surface areas and more abundant pores than the latter. Meanwhile, PTC shows a typical Langmuir I type adsorption-desorption isotherm while PTAC- x display I/IV-type isotherms. Compared with PTC, PTAC- x shows a much wider step in the P/P_0 range of $0\text{--}0.40$, suggesting the existence of micro- and mesopores. Furthermore, as for PTAC- x ($x = 6$ and 8), the N_2 adsorption volume increases slightly with the increase of relative pressure in the range of $0.40\text{--}0.85$, implying the existence of mesopores. Micropores are mainly originated from the KOH chemical activation. The reactions are as follows (Eqs. (1)–(6)):



Furthermore, the amount and the size of micropores increase with the increasing KOH dosage, and those mutual superimposed micropores are incorporated to develop new mesopores. The pore size distributions reveal that PTC shows only very weak intensity in the range of $2.5\text{--}4.5\text{ nm}$. While PTAC- x exhibit a much wider size distribution with high intensity (Fig. 6b). The hierarchical pores are especially favorable for energy storage of EDLC since the micropores may be used as the locations for charge accommodation and the mesopores may serve as channels to promote the rapid diffusion and transmission of ions in the interior of carbon materials

As summarized in Table 1, the specific surface areas (S_{BET}) of PTAC- x are much larger than that of PTC ($173.0\text{ m}^2\text{ g}^{-1}$) and the S_{BET} increases with x increment to some extent due to the formation of pores by KOH activation. The S_{BET} of PTAC-6 ($2670.8\text{ m}^2\text{ g}^{-1}$) is much higher than those of PTAC-2 ($1657.6\text{ m}^2\text{ g}^{-1}$) and PTAC-8 ($1976.4\text{ m}^2\text{ g}^{-1}$). This is because the excessive activation by high KOH dosage causes the collapse of etching pores, which leads to the decrease of specific surface area. Meanwhile, the total pore volume of PTAC-6 ($1.41\text{ cm}^3\text{ g}^{-1}$) is also higher than those of PTAC-8 ($0.939\text{ cm}^3\text{ g}^{-1}$), PTAC-2 ($0.717\text{ cm}^3\text{ g}^{-1}$), and PTC ($0.070\text{ cm}^3\text{ g}^{-1}$). The unique textural characteristic of PTAC-6 favors the enhancement of electrolyte ions contraction and accumulating. As a result, the charge storage density can be improved.

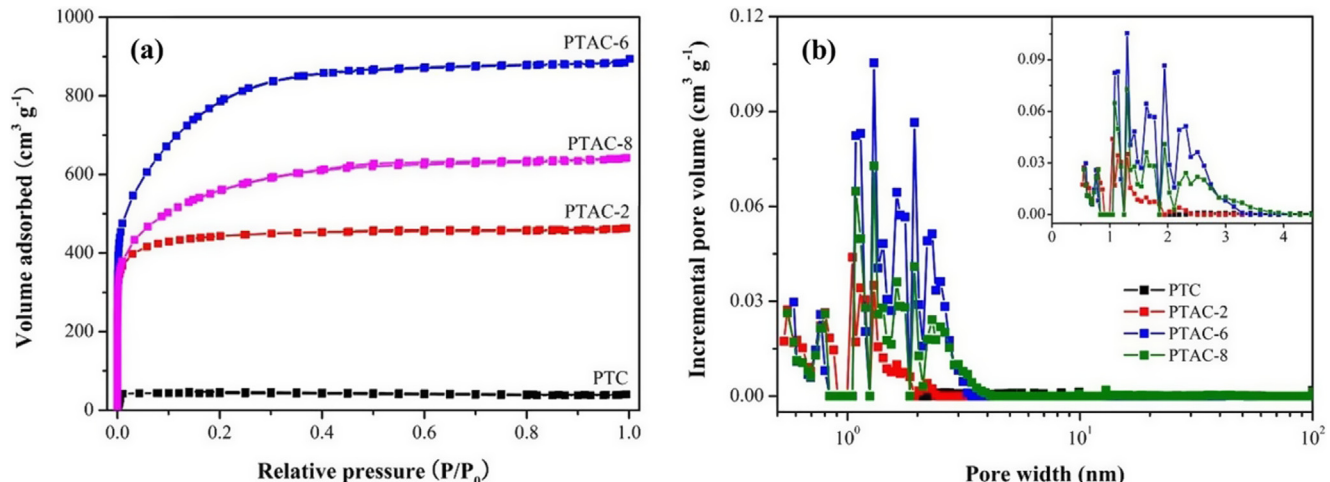


Fig. 6. N_2 adsorption-desorption isotherms (a) and pore size distributions (b) of PTC and PTAC- x .

Table 1
Textural and structural characteristics of the resultant materials.

Material	$S_{\text{BET}}^{\text{a}}$ ($\text{m}^2\text{ g}^{-1}$)	S_M^{b} ($\text{m}^2\text{ g}^{-1}$)	S_{Ex}^{c} ($\text{m}^2\text{ g}^{-1}$)	V_p^{d} ($\text{cm}^3\text{ g}^{-1}$)	V_M^{e} ($\text{cm}^3\text{ g}^{-1}$)
PTC	173.6	–	–	0.063	0.070
PTAC-2	1657.6	1361.1	296.6	0.717	0.555
PTAC-6	2670.8	368.0	2302.8	1.41	0.203
PTAC-8	1976.4	797.6	1178.8	0.993	0.348

^a S_{BET} , specific surface area calculated by the BET method.

^b S_M , micropore area calculated by the V-t method (t-plot method micropore analysis).

^c S_{Ex} , external surface area calculated by the V-t method (t-plot method micropore analysis).

^d V_p , total pore volume determined by N_2 adsorption at a relative pressure of 0.99.

^e V_M , micropore volume calculated by the V-t method (t-plot method micropore analysis).

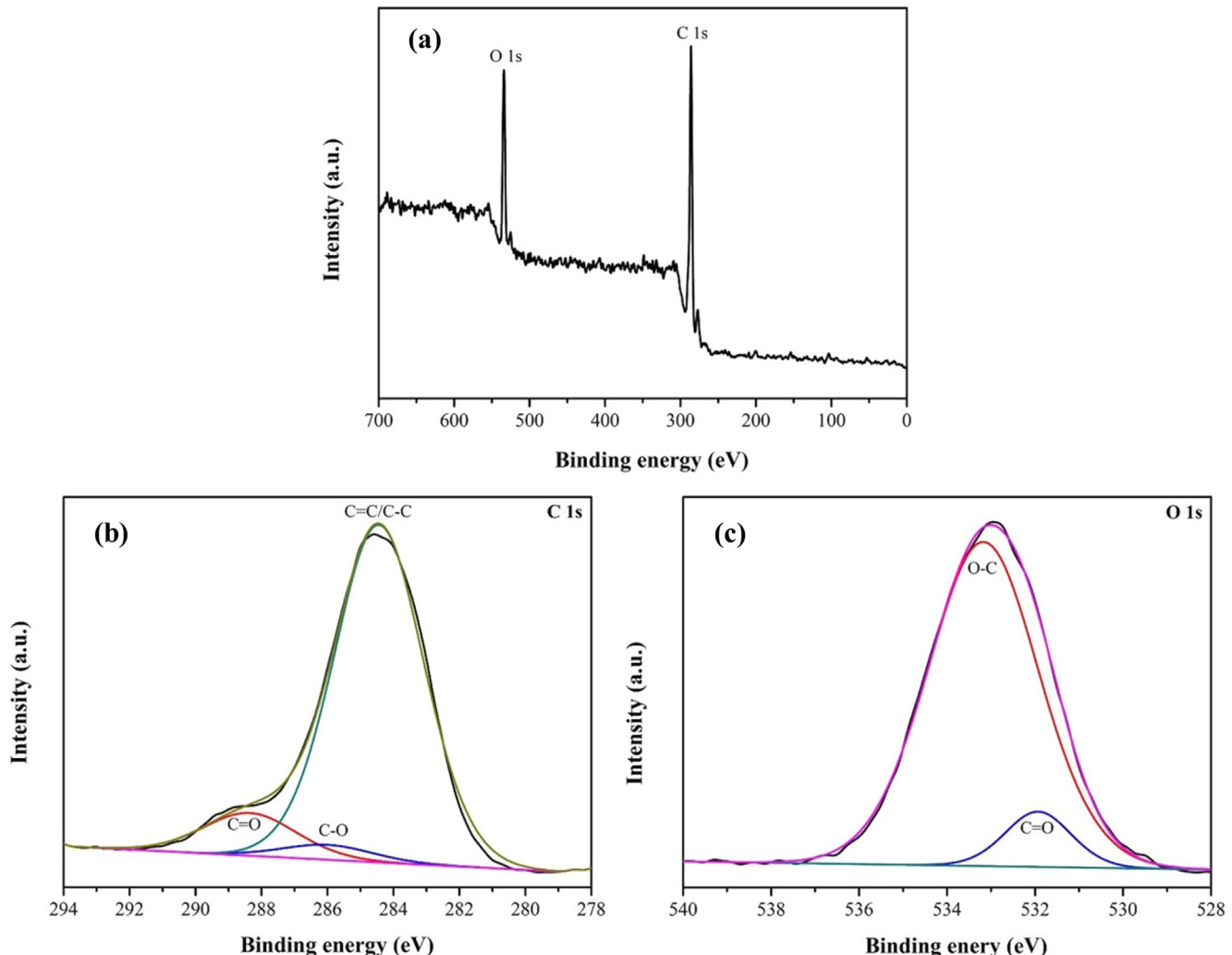


Fig. 7. XPS survey spectrum (a), high-resolution C 1s (b) and O 1s (c) spectra of PTAC-6.

XPS measurement is employed to investigate the chemical bonding information on PTAC-6 surface. The survey scan spectrum shown in Fig. 7a exhibits that the material contains only two elements including carbon (81.5 at.%) and oxygen (18.5 at.%). The C 1s XPS spectrum of PTAC-6 can be deconvoluted into three-type peaks appeared at 284.6 eV, 286.6 eV, and 288.4 eV (Fig. 7b), which are ascribed to C=C/C-C, C—O, and C=O, respectively [27]. The high-resolution O 1s spectrum shown in Fig. 7c could be deconvoluted into two peaks attributed to C=O (532.2 eV) and C—O (533.5 eV), respectively [28]. Compared with the carbon-carbon groups, these oxygen-functional groups can improve the wettability of the electrolyte (KOH), resulting in increasing utilization of the surface area and improving ion transport properties at high current densities [27,28]. Therefore, the cotonier strobili fibers-derived carbon is expected to exhibit surpassing capacitive performance when used as electrode materials for EDLCs.

3.2. Electrochemical performance

A three-electrode supercapacitor system is used to evaluate the electrochemical properties of PTC and PTAC-x. Fig. 8a shows their CV curves at 100 mV s⁻¹. Differ from PTC, the resultant PTAC-x materials exhibit a quasi-rectangular shape in the range of -1.0

to 0 V, indicating their ideal capacitive performance. The current densities at low potential reign are higher than those at high potential reign for all the materials. This is attributed to the redox reactions caused by the oxygen-functional groups on the carbon surfaces involved the decomposing of the electrolyte to H₂ and/or O₂ evolution [29–37]. Furthermore, PTAC-6 displays the largest CV curve area among the materials, indicating it possesses the largest capacitance in terms of its high specific surface area and suitable pore size distribution as mentioned above. The CV curves for PTAC-6 retain nearly symmetric and rectangular-like shape when the potential scan rate varies in the range of 5–100 mV s⁻¹ (Fig. 8b), demonstrating the fast kinetics for the formation of electrical double-layer, good rate capability, and low internal resistance.

All the GCD curves for PTC and PTAC-x at 1 A g⁻¹ shown in Fig. 8c display the quasi-line appearance, suggesting their both EDLC and pseudo-capacitive behaviors. It is widely accepted that the discharge time has close connection with the specific capacitance. PTAC-6 shows the longest discharge time, indicating PTAC-6 has a higher capacitance than the others. This is consistent with the aforementioned CV results. As discussed above, the high specific area and abundant micropores & mesopores of PTAC-6 are beneficial to improve the contacting and accumulating more

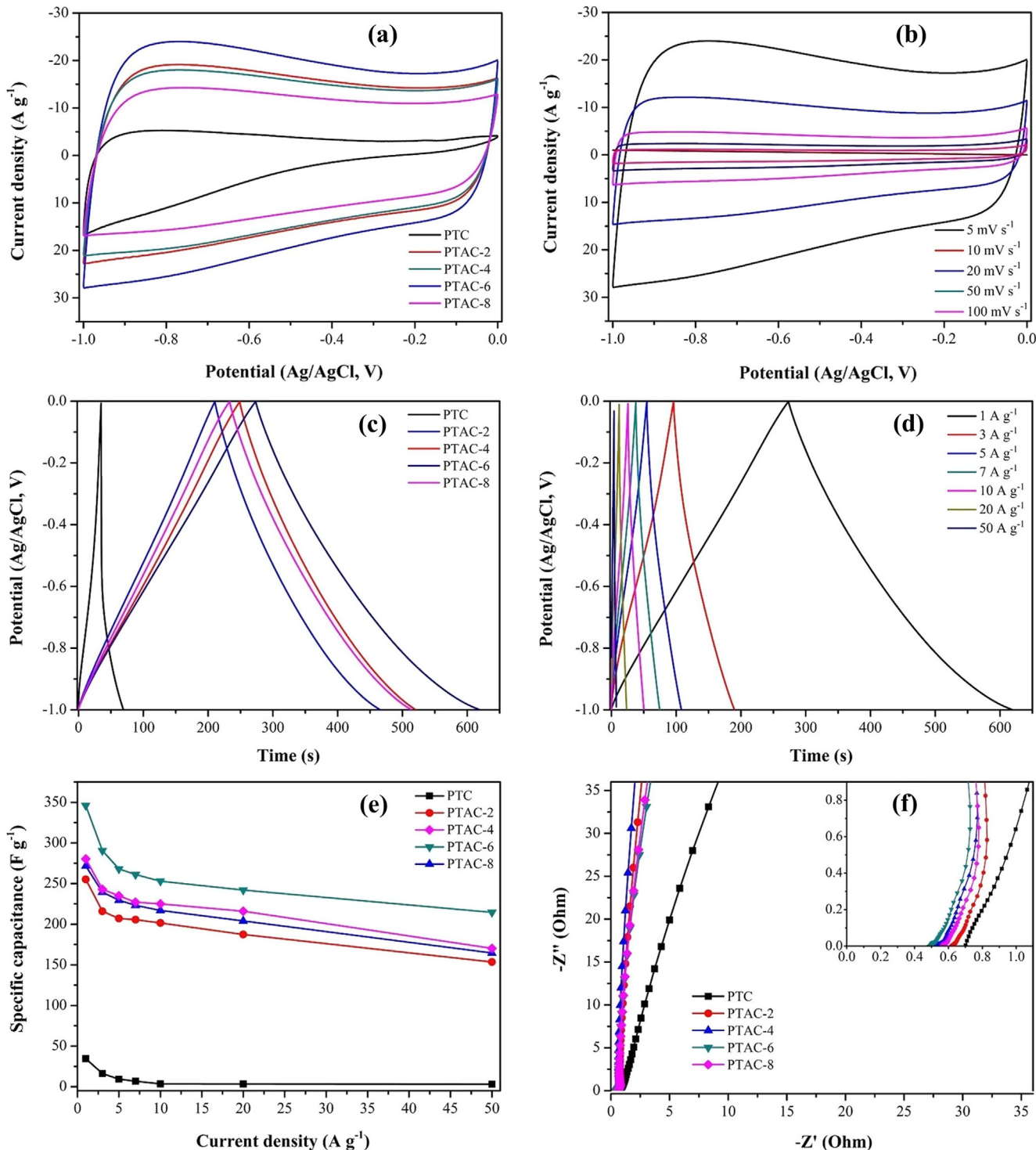


Fig. 8. Electrochemical performance of PTC and PTAC-x in the three-electrode system: (a) CV curves for PTC and PTAC-x at 100 mV s^{-1} ; (b) CV curves for PTAC-6 at various scan rates; (c) GCD curves for PTC and PTAC-x at 1 A g^{-1} ; (d) GCD curves for PTAC-6 at various current densities; (e) Specific capacitances of PTC and PTAC-x at different current densities; (f) Nyquist plots for PTC and PTAC-x.

electrolyte ions, leading to high charge storage density. Meanwhile, these mesopores facilitate the fast diffusion of KOH ions in their pore channels at high current densities.

Fig. 8d also shows the isosceles triangle-like GCD curves of PTAC-6 at the range of $1\text{--}50 \text{ A g}^{-1}$. It can be seen that the charge/discharge time decreases with the increase of current density. This

is because the electrolyte ions need more time to penetrate and diffuse into the electrode pores at lower current densities than higher current densities. The specific capacitance of PTAC-6 is 346.1 F g^{-1} at 1 A g^{-1} . The more detailed specific capacitances of PTAC-6 are calculated to be $290.5, 268.0, 261.2, 253.0, 242.0$, and 214.5 F g^{-1} at $3, 5, 7, 10, 20$, and 50 A g^{-1} , respectively. Signifi-

Table 2

Comparison on specific capacitances of different biomass-based electrodes.

Biomass	C_g ($F\ g^{-1}$) (current density)	Electrolyte	Ref.
Ginkgo leaves	302 ($1\ A\ g^{-1}$)	6 M KOH	[15]
Poplar catkins	314.6 ($1\ A\ g^{-1}$)	6 M KOH	[18]
Corn cob	328.4 ($0.5\ A\ g^{-1}$)	6 M KOH	[19]
Rice husk ash	260 ($1\ A\ g^{-1}$)	6 M KOH	[20]
Willow catkins	306 ($0.1\ A\ g^{-1}$)	6 M KOH	[21]
Willow catkins	292 ($1\ A\ g^{-1}$)	6 M KOH	[23]
Tobacco rods	286.6 ($0.5\ A\ g^{-1}$)	6 M KOH	[24]
Bamboo	188 ($1\ A\ g^{-1}$)	1 M KOH	[25]
Potato waste residue	255 ($0.5\ A\ g^{-1}$)	2 M KOH	[26]
Pomelo peel	342 ($1\ A\ g^{-1}$)	2 M KOH	[29]
Cotton	189.8 ($1\ A\ g^{-1}$)	3 M KOH	[30]
Cattail	126.5 ($0.5\ A\ g^{-1}$)	6 M KOH	[31]
Acacia gum	272 ($1\ A\ g^{-1}$)	6 M KOH	[32]
Pomelo peel	207.4 ($1\ A\ g^{-1}$)	6 M KOH	[33]
Auriculiformis tree bark	191 ($1\ A\ g^{-1}$)	1 M Na ₂ SO ₄	[34]
Agaric	292 ($1\ A\ g^{-1}$)	6 M KOH	[35]
Shiitake mushroom	306 ($1\ A\ g^{-1}$)	6 M KOH	[36]
Cotonier strobili fibers	346.1 ($1\ A\ g^{-1}$)	6 M KOH	Our work

cantly, the specific capacitance of PTAC-6 ($346.1\ F\ g^{-1}$ at $1\ A\ g^{-1}$) is obviously higher than that of the previously reported ACs (Table 2).

Fig. 8e exhibits the specific capacitance of PTC and PTAC-x at different current densities. Notably, the capacitance of PTAC-6 is much higher than that of others in the wide range of current densities (1 – $50\ A\ g^{-1}$) with a retention ratio of 62.0%. This is much better than those of PTC (8.7%) and other PTAC-x materials (60.1–60.7%), implying that dosage of KOH is important for improving the capacitive performance.

EIS is further applied to make a thorough inquiry into the charge transfer resistance of PTC and PTAC-x electrodes. The Nyquist plots include two main parts: a semicircle at the high frequency region and a straight line in the low frequency range. The small semicircles in Fig. 8f inset reflect the low charge transfer resistance (R_{ct}) and the intercept of the semicircle at Z_0 axis indicate the equivalent series resistance (R_s). Significantly, PTAC-6 has a smaller R_{ct} and R_s than the others, indicating it has higher electrical conductivity and lower contact resistance. Moreover, as depicted in Fig. 8f, a nearly vertical straight line for PTAC-6 suggests a fast charge diffusion and storage in the electrode materials.

The effect of calcination temperatures of PTAC-6 on the capacitive performance is also considered (Fig. 9). Compared with other

temperatures, the material calcined at $800\ ^\circ C$ exhibits the largest CV curve area and the longest discharge time. These results confirm that $800\ ^\circ C$ is the optimized calcination temperature for the chemical activation of PTC with KOH under the present condition.

Based on the above results, PTAC-6 demonstrates the superior capacitive performance in terms of high capacitance and high-rate capability. A PTAC-6-based symmetric supercapacitor was constructed to further evaluate the practical viability. The CV curves at $50\ mV\ s^{-1}$ with different potential range display the nearly rectangular and symmetric shapes, indicating an ideal capacitive behavior combined without any obvious redox peak even when the voltage is as high as $1.6\ V$ (Fig. 10a). Moreover, the CV curves recorded at the range of 5 – $100\ mV\ s^{-1}$ revealing an almost symmetric rectangular shape (Fig. 10b). This is a dominant EDLC behavior.

The GCD curves of the PTAC-6 symmetric cell at various current densities (0.2 – $10\ A\ g^{-1}$) are shown in Fig. 10c. These nearly linear and symmetrical curves with a slight curvature indicate the good capacitive behavior of EDLC with a portion of pseudocapacitance, which is ascribed to the influence of the oxygen groups in PTAC-6 as mentioned above. At low charging rate, the electrolyte may diffuse through entire micro- and mesopores thereby the specific capacitance could be improved significantly. While the electrolyte can only access the mesoporous at higher charging rates, which in turn reduces the specific capacitance [38,39]. The decrease of specific capacitance could be attributed to the less protons diffusion and migration through the electrodes because of the high current density and limited volume. The initially specific capacitance retention of 59.3% is achieved at $10\ A\ g^{-1}$ (Fig. 10d). The decrease could be attributed to the diffusion and migration of few protons through the electrodes because of the high current density and limited volume. The value of Ohmic resistance (R_0) is around $2.51\ \Omega$ in the Nyquist plots for the resultant symmetric supercapacitors (Fig. 10e). The low R_{ct} and short Warburg region at the 45° sloped curves in Fig. 10e inset indicate the efficient charge transfer process in the PTAC-6 electrode. Fig. 10f exhibits the Ragone plot of the symmetric supercapacitor. It is noted that a maximum energy density of $33.0\ Wh\ kg^{-1}$ is obtained at $160.0\ W\ kg^{-1}$, which can still be retained as $19.6\ Wh\ kg^{-1}$ at a high power density of $8106.7\ W\ kg^{-1}$. More importantly, the energy density is comparable to or even higher than most of the other biomass-derived carbons listed in Table 3. Additionally, the symmetric capacitor exhibits excellent cycling stability. Its capacitance retention is as high as 84.21% and the columbic efficiency maintains around 100% after 10,000 cycles

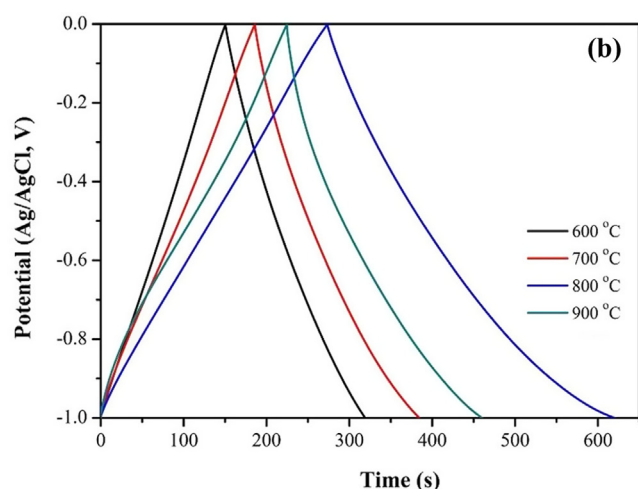
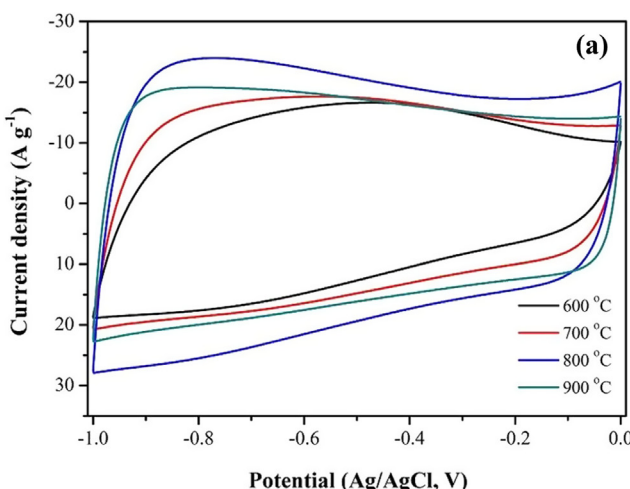


Fig. 9. CV curves at $100\ mV\ s^{-1}$ (a) and GCD curves at $1\ A\ g^{-1}$ (b) for PTAC-6 calcined at various temperatures in the three-electrode system.

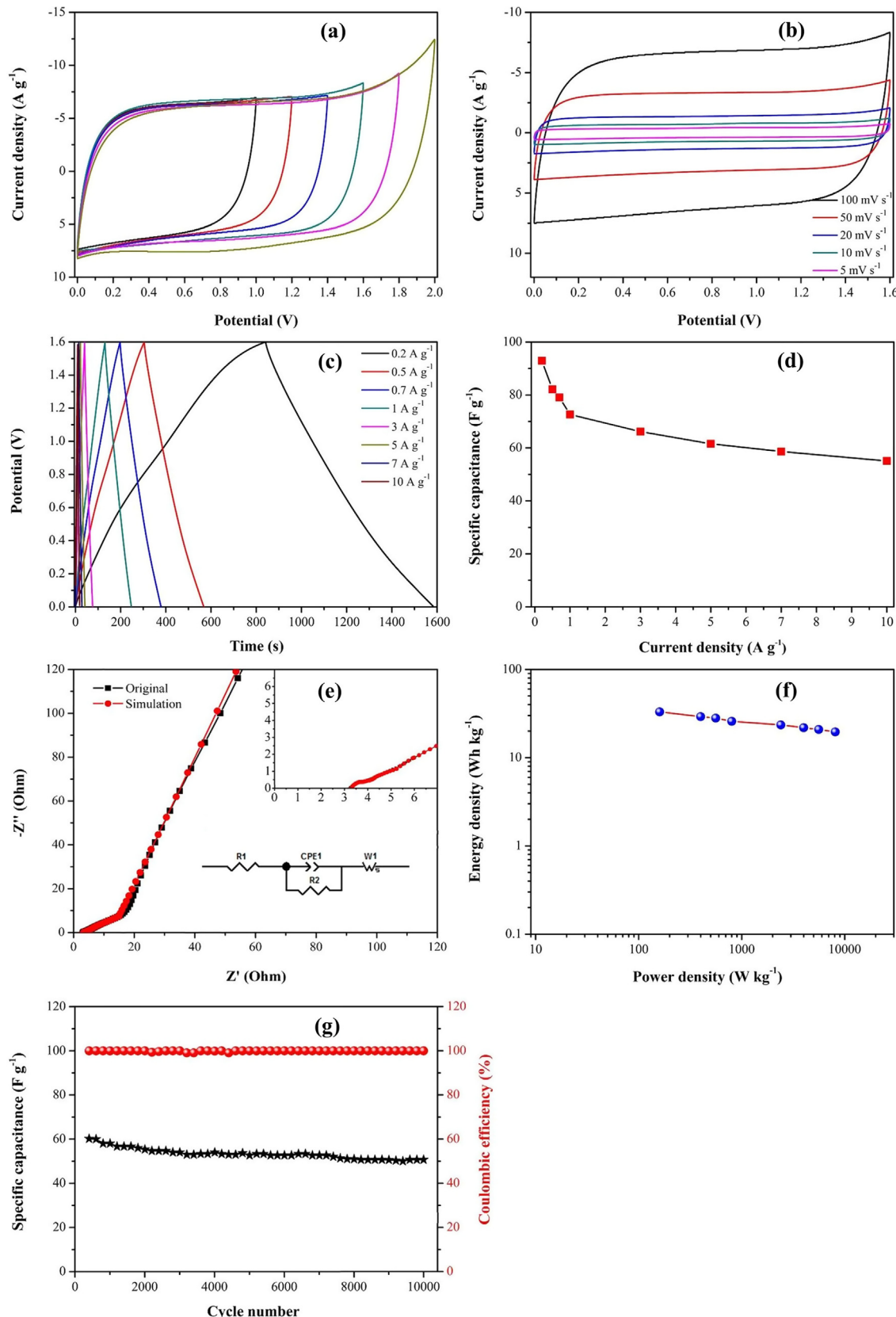


Fig. 10. Electrochemical performance of PTAC-6 in the two-electrode system: (a) CV curves at 100 mV s^{-1} ; (b) CV curves at various scan rates; (c) GCD curves at different current densities; (d) Specific capacitance at different current densities; (e) Nyquist plots; (f) The Ragone plots; and (g) The specific capacitance retention and columbic efficiency at 1 A g^{-1} .

Table 3

Comparison of energy density and power density of various biomass-derived carbon materials.

Biomass	Energy density (E, Wh kg ⁻¹)	Power density (P, W kg ⁻¹)	Ref.
Ginkgo leaves	16.0	50,000	[10]
Elm samara	25.4	15,000	[16]
Poplar catkins	20.9	180.1	[18]
Willow catkins	37.9	700	[23]
Pomelo peel	17.1	3854	[29]
Cotton stalk	18.14	450.37	[32]
Bacterial cellulose	33	36,800	[40]
Corn husk	21	875	[41]
Quercus suber	18.6	449.4	[42]
Reed	11.4	98,000	[43]
Seedpods	11.8	12.5	[44]
Cornstalk	20.2	398	[45]
Batata leaves and stalks	24.5	12,918.0	[46]
Cotonier strobili fibers	33.04	160	Our work

between 0 and 1.6 V at 1 A g⁻¹ (Fig. 10 g). The above results clearly confirm the good rate performance of PTAC-6-based symmetric supercapacitor.

4. Conclusions

The biomass waste-cotonier strobili fibers are used to prepare hierarchical porous carbon tubes (PTAC-x) activated by KOH. The resultant carbon materials possess high accessible surface area and abundant micro-mesometer level pores, which benefit large-scale ion storage and high-rate ion transfer. The optimized supercapacitor electrode material, denoted as PTAC-6, exhibits a superior high specific capacitance of 346.1 F g⁻¹ at 1 A g⁻¹ in the three-electrode supercapacitor. Furthermore, PTAC-6 shows a high energy density of 33.04 Wh kg⁻¹ at 160 W kg⁻¹ and excellent cycling stability in a coin-type symmetric supercapacitor. Such porous carbon tube materials derived from the low-cost, sustainable and abundant cotonier strobili fiber bio-wastes demonstrate a substantial potential for energy storage applications such as supercapacitors or even Li-ion batteries.

Acknowledgements

Financial supports from the National Natural Science Foundation of China (No. U1304203), the Natural Science Foundation of Henan Province (No. 162300410258), the Foundation of Henan Educational Committee (No. 16A150046), the College Science and Technology Innovation Team of Henan Province (No. 16IRTSTHN001), and 111 Project (B12015) are greatly acknowledged.

References

- Z. Wu, L. Li, J.M. Yan, X.B. Zhang, Materials design and system construction for conventional and new-concept supercapacitors, *Adv. Sci.* 4 (2017) 1600382.
- K. Xiang, Z.C. Xu, T.T. Qu, Z.F. Tian, Y. Zhang, Y.Z. Wang, M.J. Xie, X.K. Guo, W.P. Ding, X.F. Guo, Two dimensional oxygen-vacancy-rich Co₃O₄ nanosheets with excellent supercapacitor performances, *Chem. Commun.* 53 (2017) 12410–12413.
- X.Y. Zhang, P. Samori, Graphene/polymer nanocomposites for supercapacitors, *Chemnanomat* 3 (2017) 362–372.
- Q.F. Meng, K.F. Cai, Y.X. Chen, L.D. Chen, Research progress on conducting polymer based supercapacitor electrode materials, *Nano Energy* 36 (2017) 268–285.
- A. Afzal, F.A. Abuilaiwi, A. Habib, M. Awais, S.B. Waje, M.A. Atieh, Polypyrrole/carbon nanotube supercapacitors: technological advances and challenges, *J. Power Sources* 352 (2017) 174–186.
- J.Y. Liang, C.C. Wang, S.Y. Lu, Glucose-derived nitrogen-doped hierarchical hollow nest-like carbon nanostructures from a novel template-free method as an outstanding electrode material for supercapacitors, *J. Mater. Chem. A* 3 (2015) 24453–24462.
- M. Wei, F. Zhang, W. Wang, P. Alexandridis, C. Zhou, G. Wu, 3D direct writing fabrication of electrodes for electrochemical storage devices, *J. Power Sources* 354 (2017) 134–147.
- J.Y. Liang, J.X. Zhao, Y.X. Li, K.T. Lee, C. Liu, H. Lin, Q. Cheng, Q. Lan, L.F. Wu, S. Tang, L. An, Y.C. Cao, In situ SiO₂ etching strategy to prepare rice husk-derived porous carbons for supercapacitor application, *J. Taiwan Inst. Chem. E* 81 (2017) 383–390.
- N.N. Guo, M. Li, Y. Wang, X.K. Sun, F. Wang, R. Yang, Soybean root-derived hierarchical porous carbon as electrode material for high-performance supercapacitors in ionic liquids, *ACS Appl. Mater. Interf.* 8 (2016) 33626–33634.
- E.C. Hao, W. Liu, S. Liu, Y. Zhang, H.L. Wang, S.G. Chen, F.L. Cheng, S.P. Zhao, H.Z. Yang, Rich sulfur doping porous carbon materials derived from ginkgo leaves for multiple electrochemical energy storage, *J. Mater. Chem. A* 5 (2017) 2204–2214.
- J.L. Goldfarb, G.L. Dou, M. Salari, M.W. Grinstaff, Biomass-based fuels and activated carbon electrode materials: An integrated approach to green energy systems, *ACS Sustain. Chem. Eng.* 5 (2017) 3046–3054.
- H.X. Li, Y. Gong, C.P. Fu, H.H. Zhou, W.J. Yang, M.L. Guo, M.B. Li, Y.F. Kuang, A novel method to prepare nanotubes@mesoporous carbon composite material based on waste biomass and its electrochemical performance, *J. Mater. Chem. A* 5 (2017) 3875–3887.
- J.Y. Liang, T.T. Qu, X. Kun, Y. Zhang, S.Y. Chen, Y.C. Cao, M.J. Xie, X.F. Guo, Microwave assisted synthesis of camellia oleifera shell-derived porous carbon with rich oxygen functionalities and superior supercapacitor performance, *Appl. Surf. Sci.* 436 (2018) 934–940.
- P.W. Xiao, Q.H. Meng, L. Zhao, J.J. Li, Z.X. Wei, B.H. Han, Biomass-derived flexible porous carbon materials and their applications in supercapacitor and gas adsorption, *Mater. Design* 129 (2017) 164–172.
- H.J. An, N.R. Kim, M.Y. Song, Y.S. Yun, H.J. Jin, Fallen-leaf-derived microporous pyropolymers for supercapacitors, *J. Ind. Eng. Chem.* 45 (2017) 223–228.
- C. Chen, D.F. Yu, G.Y. Zhao, B.S. Du, W. Tang, L. Sun, Y. Sun, F. Besenbacher, M. Yu, Three-dimensional scaffolding framework of porous carbon nanosheets derived from plant wastes for high-performance supercapacitors, *Nano Energy* 27 (2016) 377–389.
- H.B. Feng, H. Hu, H.W. Dong, Y. Xiao, Y.J. Cai, B.F. Lei, Y.L. Liu, M.T. Zheng, Hierarchical structured carbon derived from bagasse wastes: a simple and efficient synthesis route and its improved electrochemical properties for high-performance supercapacitors, *J. Power Sources* 302 (2016) 164–173.
- X.L. Su, M.Y. Cheng, L. Fu, J.H. Yang, X.C. Zheng, X.X. Guan, Superior supercapacitive performance of hollow activated carbon nanomesh with hierarchical structure derived from poplar catkins, *J. Power Sources* 362 (2017) 27–38.
- D.B. Wang, Z. Geng, B. Li, C.M. Zhang, High performance electrode materials for electric double-layer capacitors based on biomass-derived activated carbons, *Electrochim. Acta* 173 (2015) 377–384.
- Y.Q. Huang, J. He, Y.T. Luan, Y. Jiang, S.E. Guo, X.G. Zhang, C.G. Tian, B.J. Jiang, Promising biomass-derived hierarchical porous carbon material for high performance supercapacitor, *RSC Adv.* 7 (2017) 10385–10390.
- K. Wang, R. Yan, N. Zhao, X.D. Tian, X. Li, S.W. Lei, Y. Song, Q.G. Guo, L. Liu, Bio-inspired hollow activated carbon microtubes derived from willow catkins for supercapacitors with high volumetric performance, *Mater. Lett.* 174 (2016) 249–252.
- K. Wang, N. Zhao, S.W. Lei, R. Yan, X.D. Tian, J.Z. Wang, Y. Song, D.F. Xu, Q.G. Guo, L. Liu, Promising biomass-based activated carbons derived from willow catkins for high performance supercapacitors, *Electrochim. Acta* 166 (2015) 1–11.
- L.J. Xie, G.H. Sun, F.Y. Su, X.Q. Guo, Q.Q. Kong, X.M. Li, X.H. Huang, L. Wan, W. Song, K.X. Li, C.X. Lv, C.M. Chen, Hierarchical porous carbon microtubes derived from willow catkins for supercapacitor applications, *J. Mater. Chem. A* 4 (2016) 1637–1646.
- Y.Q. Zhao, M. Lu, P.Y. Tao, Y.J. Zhang, X.T. Gong, Z. Yang, G.Q. Zhang, H.L. Li, Hierarchically porous and heteroatom doped carbon derived from tobacco rods for supercapacitors, *J. Power Sources* 307 (2016) 391–400.
- H. Chen, D. Liu, Z.H. Shen, B.F. Bao, S.Y. Zhao, L.M. Wu, Functional biomass carbons with hierarchical porous structure for supercapacitor electrode materials, *Electrochim. Acta* 180 (2015) 241–251.
- G.F. Ma, Q. Yang, K.J. Sun, H. Peng, F.T. Ran, X.L. Zhao, Z.Q. Lei, Nitrogen-doped porous carbon derived from biomass waste for high-performance supercapacitor, *Bioresource. Technol.* 197 (2015) 137–142.
- J.N. Yi, Y. Qing, C.T. Wu, Y.X. Zeng, Y.Q. Wu, X.H. Lu, Y.X. Tong, Ligno cellulose-derived porous phosphorus-doped carbon as advanced electrode for supercapacitors, *J. Power Sources* 351 (2017) 130–137.
- D.Y. Lee, G.H. An, H.J. Ahn, High-surface-area tofu based activated porous carbon for electrical double-layer capacitors, *J. Ind. Eng. Chem.* 52 (2017) 121–127.
- C. Peng, J.W. Lang, S. Xu, X.L. Wang, Oxygen-enriched activated carbons from pomelo peel in high energy density supercapacitor, *RSC Adv.* 4 (2014) 54662–54667.
- Y. Liu, Z.J. Shi, Y.F. Gao, W.D. An, Z.Z. Cao, J.R. Liu, Biomass-swelling assisted synthesis of hierarchical porous carbon fibers for supercapacitor electrodes, *ACS Appl. Mater. Interf.* 8 (2016) 28283–28290.
- M. Yu, Y.Y. Han, J. Li, L.J. Wang, CO₂-activated porous carbon derived from cattail biomass for removal of malachite green dye and application as supercapacitors, *Chem. Eng. J.* 317 (2017) 493–502.

- [32] Y. Fan, P.F. Liu, B. Zhu, S.F. Chen, K.L. Yao, R. Han, Microporous carbon derived from acacia gum with tuned porosity for high-performance electrochemical capacitors, *Int. J. Hydrogen Energy* 40 (2015) 6188–6196.
- [33] J. Li, W.L. Liu, D. Xiao, X.H. Wang, Oxygen-rich hierarchical porous carbon made from pomelo peel fiber as electrode material for supercapacitor, *Appl. Surf. Sci.* 416 (2017) 918–924.
- [34] D. Momodu, M. Madito, F. Barzegar, A. Bello, A. Khaleed, O. Olaniyan, J. Dangbegnon, N. Manyala, Activated carbon derived from tree bark biomass with promising material properties for supercapacitors, *J. Solid State Electron.* 21 (2017) 859–872.
- [35] R. Zang, S.T. Zhang, C. Li, Preparation of fungi-based activated carbon and its supercapacitive performance, *New Chem. Mater.* 45 (2017) 68–70.
- [36] P. Cheng, S.Y. Gao, P.Y. Zang, X.F. Yang, Y.L. Bai, H. Xu, Z.H. Liu, Z.B. Lei, Hierarchically porous carbon by activation of shiitake mushroom for capacitive energy storage, *Carbon* 93 (2015) 315–324.
- [37] G.F. Ma, F.T. Hua, K.J. Sun, Z.G. Zhang, E.K. Feng, H. Peng, Z.Q. Lei, Porous carbon derived from sorghum stalk for symmetric supercapacitor, *RSC Adv.* 6 (2016) 103508–103516.
- [38] N. Sudhan, K. Subramani, M. Karnan, N. Ilayaraja, M. Sathish, Biomass-derived activated porous carbon from rice straw for high energy symmetric supercapacitor in aqueous and non-aqueous electrolytes, *Energy Fuel* 3 (2017) 977–985.
- [39] Y.G. Wang, Y.F. Song, Y.Y. Xia, Electrochemical capacitors: mechanism, materials, systems, characterization and applications, *Chem. Soc. Rev.* 45 (2016) 5925–5950.
- [40] D.D. Shan, J. Yang, W. Liu, J. Yan, Z.J. Fan, Biomass-derived three-dimensional honeycomb-like hierarchical structured carbon for ultrahigh-energy-density asymmetric supercapacitors, *J. Mater. Chem. A* 4 (2016) 13589–13602.
- [41] S.J. Song, F.W. Ma, G. Wu, D. Ma, W.D. Geng, J.F. Wan, Facile self-template large scale preparation of biomass-derived 3D hierarchical porous carbon for advanced supercapacitors, *J. Mater. Chem. A* 3 (2015) 18154–18162.
- [42] F.O. Ochaj-Ejeh, A. Bello, J. Dangbegnon, A.A. Khaleed, M.J. Madito, F. Bazegar, N. Manyala, High electrochemical performance of hierarchical porous activated carbon derived from lightweight cork (*Quercus suber*), *J. Mater. Sci.* 52 (2017) 10600–10613.
- [43] D. Zhou, H.L. Wang, N. Mao, Y.R. Chen, Y. Zhou, T.P. Yin, H. Xie, W. Liu, S.G. Chen, X. Wang, High energy supercapacitors based on interconnected porous carbon nanosheets with ionic liquid electrolyte, *Micropor. Mesopor. Mater.* 241 (2017) 202–209.
- [44] Q.X. Xie, G.H. Chen, R.R. Bao, Y.F. Zhang, S.F. Wu, Polystyrene foam derived nitrogen-enriched porous carbon/graphene composites with high volumetric capacitances for aqueous supercapacitors, *Micropor. Mesopor. Mater.* 239 (2017) 130–137.
- [45] H. Yu, W.L. Zhang, T. Li, Capacitive performance of porous carbon nanosheets derived from biomass cornstalk, *RSC Adv.* 7 (2017) 1067–1074.
- [46] X.J. Wei, Y.B. Li, S.Y. Gao, Biomass-derived interconnected carbon nanoring electrochemical capacitors with high performance in both strongly acidic and alkaline electrolytes, *J. Mater. Chem. A* 5 (2017) 181–188.